INTERNATIONAL JOURNAL FOR NUMERICAL METHODS IN FLUIDS
Int. J. Numer. Meth. Fluids 2002; **39**:919–937 (DOI: 10.1002/fld.352)

Large eddy simulation of free surface turbulent flow in partly vegetated open channels

Su Xiaohui[1] and C. W. Li[2,*,†]

[1]*School of Civil Engineering and Architecture, Dalian University of Technology, Dalian, China*
[2]*Department of Civil and Structural Engineering, The Hong Kong Polytechnic University, Hong Kong SAR, China*

SUMMARY

A large eddy simulation (LES) model has been developed to simulate the hydrodynamic behaviour of turbulent flow in an open channel with a domain of vegetation. Vegetation is considered as an internal source of resistant force and turbulence energy. The model is modified from the LES model of Li and Wang (International Journal for Numerical Methods in Fluids 2000; **34**), and is distinctive in that the subgrid scale turbulence is parameterized by a k–l model. The length scale of turbulence l is proportional to the grid size and the turbulence energy k is obtained from the solution of the turbulence energy transport equation. An operator splitting method, which splits the solution procedure into advection, diffusion and pressure propagation steps, is employed so that different numerical schemes can be used for the solution of different physical processes. The model has been applied to simulate open channel flow with transverse shear produced by vegetation drag. Some organized large eddies were found in the interface between the vegetated and non-vegetated regions and the organized structure clearly has a life cycle. At the interface the transverse velocity profile exhibits a steep gradient, which induces significant mass and momentum exchange, acts as a source of vorticity, and generates high Reynolds stresses. The logarithmic vertical velocity variation becomes uniform in the vegetated domain. The agreement between the numerical results and the experimental data (Tsujimoto and Kitamura, *KHL Progressive Report* '92, Hydrology Laboratory, Kanazawa University, Japan, 1992; **21**) is satisfactory. The present k–l LES model is proven to be a useful tool for engineering applications, as it can simulate the dynamic development of large eddies and the associated intermittent turbulence. Copyright © 2002 John Wiley & Sons, Ltd.

INTRODUCTION

There is an increasing environmental concern about wetlands, river basins, as well as flood control channels recently. Growth of vegetation in these areas is desirable as it can provide

* Correspondence to: C. W. Li, Department of Civil & Structural Engineering, The Hong Kong Polytechnic University, Hong Kong SAR, People's Republic of China.
† E-mail: cecwli@polyu.edu.hk

Contract/grant sponsor: Research Grant Council of the Hong Kong Special Administrative Region; contract/grant number: 5048/99E

Received August 2001
Revised December 2001

favourable space for various lives. It is common that a watercourse has a vegetated region and a main flow region without vegetation. In addition to the resistance offered by the vegetation to the flow, violent transverse mixing due to the considerable difference between the velocities at the interface of the vegetated and the non-vegetated regions occurs.

Early works on flow in open channel with vegetation are summarized in References [1, 2]. The vegetation was treated as uniform boundary roughness and its resisting effect was reflected in the value of the so-called retardance coefficient. No information on flow within the obstruction was reported. Subsequent works used semi-empirical approaches. Myers and Elsawy [3] and Zheleznyakov [4] found that the flow in compound channels is affected by an intensive momentum exchange between the main channel and the adjoining shallow flood-plain zones. Pasche and Rouve [5] performed laboratory experiments and field measurements and constructed a theoretical model to study overbank flow with vegetatively roughened flood plains. They observed the existence of large-scale eddies at the interface between the vegetation zone and the main channel zone. Darby and Thorne [6] combined a simple numerical hydraulic model with empirical flow-resistance equations for gravel-bed materials and vegetation roughness elements to estimate the stage–discharge relationship of channels with bank vegetation.

The experiments by Tsujimoto and Kitamura [7] indicate that transverse mixing is caused by rather organized and low-frequency fluctuation of transverse velocity, and is in association of water-surface fluctuation. The existence of horizontal large-scale eddies at the places of sharp velocity gradient has been reported both in the field and laboratory by Tamai *et al.* [8], Fukuoka and Fujita [9], Chu *et al.* [10] and Ikeda *et al.* [11].

In parallel, studies of turbulent flow in and above plant canopies have been carried out. Measurements of flow characteristics have been made by Thom [12], Shaw *et al.* [13] and Oliver [14]. Mathematical models for the flow have been proposed by Kondo [15] and others. These models are one- or two-dimensional and use the conventional eddy viscosity or mixing length hypotheses. Higher-order closure model of turbulence was proposed by Wilson and Shaw [16]. A summary of these works can be found in Reference [17]. They concluded that the simple local-diffusion models of turbulence transport are seriously deficient.

In the water environment, Burke and Stolzenbach [18] presented a one-dimensional numerical model to predict the vertical variation of flow through and above large obstructions, with special emphasis on tidally inundated marsh grass. The model included the two-equation k–ε parameterization of the turbulent stresses. Empirical terms were introduced into the model, and calibration and verification of the model have been done.

Naot *et al.* [19] developed a steady three-dimensional flow model with an algebraic stress model (ASM) of turbulence to study the turbulent flow in compound wide rectangular open channel with vegetated domain. A phenomenological model was imbedded in the algebraic stress model with the vegetation modelled as an internal resistance that exerts drag force and produces energy of turbulence. Several new terms to account for vegetation resistance were proposed. The importance of the pattern of vegetation placement on the shading factors was highlighted. However, as the model is steady, it is unable to simulate the dynamic evolution of horizontal large-scale eddies and the influence of flow geometry on the development of shear layer with large-scale eddies may not be reproduced.

Recent progress in turbulence model of large-scale eddy simulation (LES) has enabled turbulent flows to be simulated with higher accuracy. LES approach has been performed to study the aerodynamic behaviour in and above a forest [20] and around multiple windbreaks set

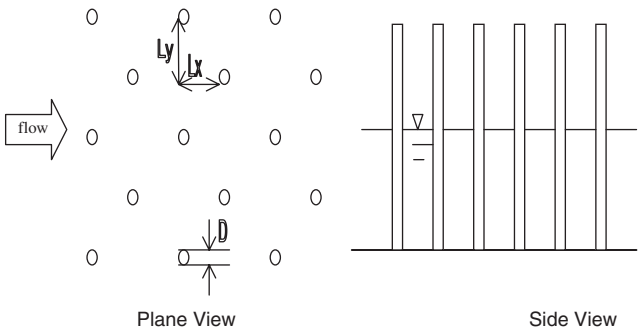

Figure 1. Illustration of the vegetation model.

within a wheat canopy [21]. Yet little has been done in open channel flow with a domain of vegetation, except that Nadaoka and Yagi [22] developed a two-dimensional depth-integrated model (SDS-2DH) to compute shallow water turbulence for flow in channel with vegetation bank. The 'subdepth scale turbulence', including the turbulence generated by the vegetation, was modelled by a k–l-type parameterization. The horizontal large-scale turbulence was computed explicitly using the technique of LES. They found that the model can account for the effects of flow geometry on the large-scale eddy development, and the model performance is better than the depth-integrated k–ε model. However, the physical reality of the computed periodic behaviour due to the lateral shift of secondary currents was questioned and the two-dimensional depth-integrated LES model is only applicable to shallow water environment with non-submerged vegetation.

In this study, a k–l LES model modified from the LES model of Li and Wang [23] has been developed to simulate the hydrodynamic behaviour of shallow turbulent flow in a rectangular open channel with a vegetated domain. The subgrid scale turbulence is modelled by a k–l model. The length scale of turbulence l is proportional to the grid size and the turbulence energy k is obtained from the solution of the turbulence energy transport equation. An operator splitting method, which splits the solution procedure into advection, diffusion and pressure propagation terms, is employed to solve the governing equations. The model will be tested against two cases of flow with vegetation for which experimental data are available.

VEGETATION DRAG FORCE AND ENERGY DISSIPATION

In physical experiments (e.g. Reference [7]), vegetation is idealized by placing vertical rods in an aligned homogeneous array, and is illustrated in Figure 1. In numerical models, the effect of these rods on the flow is modelled as internal source of resistant drag force per unit fluid mass and is added into the momentum equations [24, 25]. The expression of the resistant drag forces per unit fluid mass unit is written as

$$F_i = K\overline{u_i} \quad (i = 1, 2) \tag{1}$$

where

$$K = \tfrac{1}{2}\sqrt{\overline{u_1^2} + \overline{u_2^2} + \overline{u_3^2}}NDC_B S_F$$

$\overline{u_i}$ denotes the large-scale velocity in the x direction when $i=1$, y direction when $i=2$ and z direction when $i=3$; N is the averaged vegetation density (number of rods per unit area); D is the averaged rod diameter; C_B is the drag coefficient for flow against the rods and S_F is the shading factor.

In the present work the experimental drag coefficient C_B [26] is dependent on the Reynolds number $R = \overline{u_1}D/v$ and is approximated by

$$C_B = (10^3/R)^{0.25} \quad \text{for } R \leqslant 10^3$$

and

$$C_B = \text{minimum of } 0.976 + [(10^{-3}R - 2)/20.5]^2 \text{ or } 1.15 \quad \text{for } 10^3 < R < 4 \times 10^4$$

For aligned rods the shading factor has been determined experimentally as

$$S_F = (1 - \sqrt{D/S})^2$$

where $S = 1/\sqrt{N}$ is the averaged spacing and $\sqrt{D/S}$ is the velocity defect behind a single rod. The energy dissipation due to vegetation is written as

$$\pi_v = \frac{NDC_B S_F}{2}(\overline{u_1^2} + \overline{u_2^2} + \overline{u_3^2})^{3/2} \tag{2}$$

GOVERNING EQUATIONS

The governing equations used are the three-dimensional grid-volume-average equations describing the balances of mass and momentum under the Boussinesq approximation. The equations include additional terms for drag force produced by vegetation.

Continuity equation:

$$\frac{\partial \overline{u_i}}{\partial x_i} = 0 \quad (i = 1,2,3) \tag{3}$$

Momentum equations:

$$\frac{\partial \overline{u_i}}{\partial t} + \overline{u_j}\frac{\partial \overline{u_i}}{\partial x_j} = -\frac{1}{\rho}\frac{\partial P}{\partial x_i} + g_i + v\left(\frac{\partial^2 \overline{u_i}}{\partial x_j \partial x_j}\right) - \frac{\partial \tau_{ij}}{\partial x_j} - F_i \quad (i,j = 1,2,3) \tag{4}$$

Assuming that the pressure is hydrostatic, the momentum equation in the vertical direction $i=3$ is degenerated into the following form:

$$0 = -g_i - \frac{1}{\rho}\frac{\partial \bar{p}}{\partial x_i}, \quad i = 3 \tag{5}$$

The momentum equations include terms for subgrid-scale (SGS) fluxes, which are determined from the resolved fields and the SGS kinetic energy. The subgrid-scale model integrates a closed equation for SGS kinetic energy of the following form:

$$\frac{\partial}{\partial t}(k)+\frac{\partial}{\partial x_j}(\overline{u_j}k)=\frac{\partial}{\partial x_j}\left(\frac{v_1+v}{\sigma_k}\frac{\partial k}{\partial x_j}\right)+v_1\left(\frac{\partial \overline{u_i}}{\partial x_j}+\frac{\partial \overline{u_j}}{\partial x_i}\right)\left(\frac{\partial \overline{u_i}}{\partial x_j}+\frac{\partial \overline{u_j}}{\partial x_i}\right)+\pi_v-C_{\mathrm{D}}k^{3/2}/l$$

$$(i,j=1,2,3) \tag{6}$$

Here $\overline{u_i}$ and g_i denote the large-scale velocity component and gravity acceleration component in the ith direction, respectively, $g_1=g_2=0$; $g_3=-g$, P denotes pressure, ρ denotes density, k denotes SGS kinetic energy, v denotes molecular viscosity, C_{D} is an empirical constant and τ_{ij} denotes the SGS stress:

$$\tau_{ij}=\overline{u_i'u_j'}-\frac{1}{3}\overline{u_k'u_k'}\delta_{ij}=-v_{\mathrm{i}}\left(\frac{\partial \overline{u_i}}{\partial x_j}+\frac{\partial \overline{u_j}}{\partial x_i}\right)=-2v_{\mathrm{i}}S_{ij} \tag{7}$$

The subgrid scale eddy viscosity coefficient v_{i} is assumed to be the product of the turbulence characteristic length scale (l) and an SGS velocity scale ($k^{1/3}$):

$$v_{\mathrm{i}}=C_\mu l k^{1/2} \tag{8}$$

where C_μ is a dimensionless empirical constant ($C_\mu=0.09$) and l is defined for this problem as

$$l=C_{\mathrm{s}}\left[1-\exp\left(-\frac{y_k^+}{A^+}\right)\right](\Delta x\Delta y\Delta z)^{1/3} \tag{9}$$

where C_{s} is a constant and taken to be 0.15, l is modified by the van Driest damping with parameters y_k^+ and A^+ to account for the effect of solid wall on the suppression of eddies. $y^+=y_{\mathrm{w}}u_*/v$, y_{w} is the distance between the computing node and the wall and u_* is the friction velocity. A^+ is a constant and is equal to 26.

Free surface elevation

The vertical velocity is obtained from the continuity equation

$$\frac{\partial \overline{u_3}}{\partial x_3}=-\frac{\partial \overline{u_1}}{\partial x_1}-\frac{\partial \overline{u_2}}{\partial x_2} \tag{10}$$

The governing equation for free surface elevation can be derived from the vertical integration of the continuity equation

$$\frac{\partial \eta}{\partial t}=-\frac{\partial}{\partial x_1}\int_{-h}^{\eta}\overline{u_1}\,\mathrm{d}x_3-\frac{\partial}{\partial x_2}\int_{-h}^{\eta}\overline{u_2}\,\mathrm{d}x_3 \tag{11}$$

where $\eta(x_1,x_2)$ is the free surface elevation and $x_3=-h$ represents the bottom. The free surface elevation is related to the pressure at $x_3=0,\ P_0=P(x_1,x_2,0)$ by

$$\frac{\partial P_0}{\partial x_i}=\rho g\,\frac{\partial \eta}{\partial x_i}\quad (i=1,2) \tag{12}$$

SOLUTION METHOD

The split operator approach is used in the solution of the governing equations. At each time step the equations are split into three steps: advection, diffusion and pressure propagation. The equations for the advection step are

$$\frac{\bar{u}_i^{n+1/3}-\bar{u}_i^{n}}{\Delta t}=-\,\overline{u_j}\,\frac{\partial \overline{u_i}}{\partial x_j}\quad (i=1,2;\ j=1,2,3) \tag{13}$$

$$\frac{k^{n+1/3}-k^{n}}{\Delta t}=-\,\overline{u_j}\,\frac{\partial k}{\partial x_j}\quad (j=1,2,3) \tag{14}$$

The third-order backward characteristic scheme (Yu and Li [27], equivalent to QUICKEST, Leonard [28]) is employed to deal with the advection step in the equations. The scheme is third-order accurate and thus the second-order diffusive error is zero. The fourth-order diffusive error term of the scheme is expected to be much smaller than the second-order subgrid eddy diffusion terms.

The equations for the diffusion term are

$$\frac{\bar{u}_i^{n+2/3}-\bar{u}_i^{n+1/3}}{\Delta t}=\nu\,\frac{\partial^2 \overline{u_i}}{\partial x_j\partial x_j}-\frac{\partial(-2\nu_T S_{ij})}{\partial x_j}\quad (i=1,2;\ j=1,2,3) \tag{15}$$

$$\frac{k^{n+2/3}-k^{n+1/3}}{\Delta t}=\frac{\partial}{\partial x_j}\left(\frac{\nu}{\sigma_k}\,\frac{\partial k}{\partial x_j}\right)+\frac{\partial}{\partial x_j}\left(\frac{\nu_T}{\sigma_k}\,\frac{\partial k}{\partial x_j}\right)\quad (j=1,2,3) \tag{16}$$

In the diffusion step, the simple four-node centred space scheme is used for the second-order diffusion terms. The equations for the propagation step are

$$\frac{\eta^{n+1}-\eta^{n+2/3}}{\Delta t}=-\,\frac{\partial}{\partial x_1}\int_{-h}^{\eta}\overline{u_1}\,\mathrm{d}x_3-\frac{\partial}{\partial x_2}\int_{-h}^{\eta}\overline{u_2}\,\mathrm{d}x_3 \tag{17}$$

$$\frac{\partial \overline{u_i}}{\partial t}=-\frac{1}{\rho}\,\frac{\partial \eta}{\partial x_i}-K\overline{u_i}\quad (i=1,2) \tag{18}$$

$$\frac{k^{n+1}-k^{n+2/3}}{\Delta t}=2\nu_T\bar{S}_{ij}\bar{S}_{ij}+\pi_v-C_{\mathrm{D}}k^{3/2}/l\quad (i,j=1,2,3) \tag{19}$$

Equation (18) is due to the surface elevation not being level. Equations (17) and (18) are solved implicitly. They are decoupled through two procedures. Firstly, the unknown flow rates at time step $n+1$ are eliminated by differentiating equation (18) with respect to x and y. Secondly, the resulting Poisson-type equation with an essential boundary condition is solved by using the Gauss–Seidel iteration method. Successive over-relaxation (SOR) technique is incorporated into the Gauss–Seidel iteration method to speed up the convergence of the solution. The accepted level of reduction of the residuals on each time step is 0.1%. In the time stepping problem, the choice of acceleration method and the convergence criterion is not so significant. The solution of the Poisson-like equation takes about $\frac{2}{3}$ computer time of the whole computation.

The vertical velocity $\overline{u_3}$ is computed from the continuity equation

$$\overline{u_3} = -\int_{-h}^{\eta} \left(\frac{\partial \overline{u_1}}{\partial x_1} + \frac{\partial \overline{u_2}}{\partial x_2} \right) \mathrm{d}x_3 \tag{20}$$

For the stability criteria of the scheme, in the advection step, the criterion is given by

$$\Delta t \leqslant \min \left(\frac{\Delta X_1}{|u_{1,i,j,k}|}, \frac{\Delta X_2}{|u_{2,i,j,k}|}, \frac{\Delta X_3}{|u_{3,i,j,k}|} \right)$$

where ΔX_i is the grid size in the ith direction. In the diffusion step, the stability criterion is given by

$$\Delta t \leqslant \min \left[\frac{1}{2\nu_1} \frac{(\Delta X_1)^2 (\Delta X_2)^2 (\Delta X_3)^2}{(\Delta X_1)^2 (\Delta X_2)^2 + (\Delta X_2)^2 (\Delta X_3)^2 + (\Delta X_3)^2 (\Delta X_1)^2} \right]$$

BOUNDARY AND INITIAL CONDITIONS

Periodic boundary condition (PBC) is applied at the upstream and downstream boundaries. On the bottom, the no-slip boundary condition is used. The magnitudes of the bottom shear stresses are specified by the Manning equation. Another method of relating the bed shear stress to the near wall velocity using the log law has also been used. Results obtained by the two methods display not much difference. The log-layer solution is used in the determination of the turbulent kinetic energy near the bottom. At the lateral sidewall, similar condition as that used at the bottom is employed for the velocity and the turbulent kinetic energy. At the free surface, zero pressure is applied when the Poisson equation is solved. The continuity of stress condition imposes the zero shear and normal stresses on the free surface when wind effect is absent.

The initial condition consists of velocity, depth and turbulent kinetic energy fields. The vertical variation of the filtered longitudinal velocity $\overline{u^0_{1,i,j,k}}$ is specified as a logarithmic profile. Small disturbances, which were generated with a set of random numbers with a magnitude $<10\%$ of the mean velocity, were provided in the initial velocity field.

Table I. Physical and computational parameters for the two cases of study.

Experiment code	*CASE-1*	*CASE-2*
	Model A1	Model C1
Channel width B	40 cm	40 cm
Slope I	1.70×10^{-3}	1.65×10^{-3}
Averaged velocity U_0	32 cm/s	22 cm/s
Water depth H_0	4.57 cm	4.38 cm
Vegetation width B_s	12 cm	12 cm
Vegetation diameter D	0.02 cm	0.02 cm
Vegetation density N	30 cm^{-2}	40 cm^{-2}
Roughness n	0.012	0.012
Drag co-efficient C_B	1.988	1.53
Shade factor S_F	0.448	0.416
Longitudinal domain size	60 cm	60 cm
Longitudinal grid size	1.0 cm	1.0 cm
Transverse grid size	0.5 cm	0.5 cm
Time step	0.005 s	0.005 s

The transverse filtered velocities, $\overline{u^0_{2,i,j,k}}$ and $\overline{u^0_{3,i,j,k}}$ are assumed equal to zero. The water depth field is determined based on force balance. The initial turbulent kinetic energy field is set to zero.

MODEL ASSESSMENT

The present model has been applied to study two cases of open channel flow with vegetation in part of the domain. These cases are the replication of the physical experiments due to Tsujimoto and Kitamura [7]. The computed results will be compared with the data obtained from the experiments and the performance of the model can then be assessed. Moreover, the computed results from the depth-integrated model SDS-2DH by Nadaoka and Yagi [22] for one of the cases will be used for further comparison. The physical and computational parameters for the two cases are summarized in Table I. The definition sketch of the problem is shown in Figure 2.

The number of mesh points is $60 \times 80 \times 10$ in the streamwise, transverse and vertical directions, respectively. The shear stress is the greatest at the interface between the water and vegetation domain and its magnitude is difficult to determine. Using the bottom shear stress in the non-vegetated region, the non-dimensional grid size $u^* \Delta z/\nu = z^+ = 90$ for case 1 and $z^+ = 60$ for case 2, where Δz is the grid size in the z direction. The present grid resolution follows those used previously (e.g. Reference [20]) in similar problems. It is subsequently observed that the largest eddy is of the size approximately equal to 60 grids.

The length of simulation time in terms of the eddy turnover period is 20 for the first case and 35 for the second case. The time to development of the large eddies is approximately 10 eddy turnover periods for the first case and 25 for the second case. Flow statistics

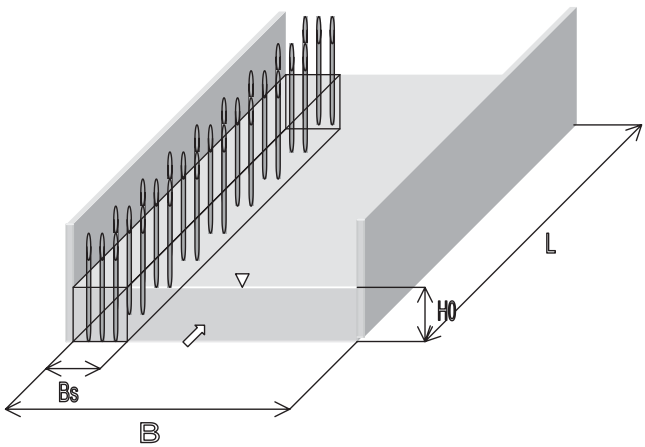

Figure 2. Definition sketch of flow with vegetation.

are collected for the last 10 eddy turnover periods for both cases. A PIII 733 PC is used and the computation time is approximately 12 h for the first case and 25 h for the second case.

Figure 3 shows the surface velocity fields of the two cases at the instant of initial development of large eddies. The corresponding vorticity field and spatial distribution of water surface are shown in Figures 4 and 5. In the computational domain one large vortex formed around the interface region between the non-vegetated and vegetated domains after the computation reaches a dynamic equilibrium state. The vortex grows in size and is then transported downstream when the size is sufficiently large. The process of generation, growing and transport of vortex is repeated in time. For case 2 the minimum vorticity computed is about $-4.0\,\mathrm{s}^{-1}$, which is the same as that computed by the SDS-2DH model. The formation of vortex also causes a decrease in pressure and hence a depression of water surface. In the computation, the initial velocity is set to the averaged velocity, which is equal to the total discharge divided by the cross-sectional area. The existence of vegetation causes the redistribution of the velocity field and the field of water surface elevation. The velocity in the vegetated domain is reduced by the presence of vegetation, also piling up of water occurs in this low-velocity region. The transverse velocity gradient therefore causes mass and momentum exchanges. This leads to hydrodynamic instability and the formation of vortex. The computed transverse velocity profile is close to that of the experiment (Figure 6).

Figure 7 shows the temporal variation of water surface fluctuation for the two cases. The mean periods of the water surface fluctuation are 2.5 and 3.4 s, respectively, which are close to the experimental results of 2.7 and 3.7 s. Figure 8 shows the transverse distribution of the root mean squares (RMS) water surface fluctuation, η_{rms}. Figure 8(b) displays the results for the present model, those of the SDS-2DH model, and those of the experiments. A surge in water level exists near the boundary of the non-vegetated region and the value of η_{rms} in the non-vegetated region is less than that in the vegetated region. In this region kinetic energy is partly converted into potential energy. Compared with the result from SDS-2DH model, the result from the present model is closer to the experiment.

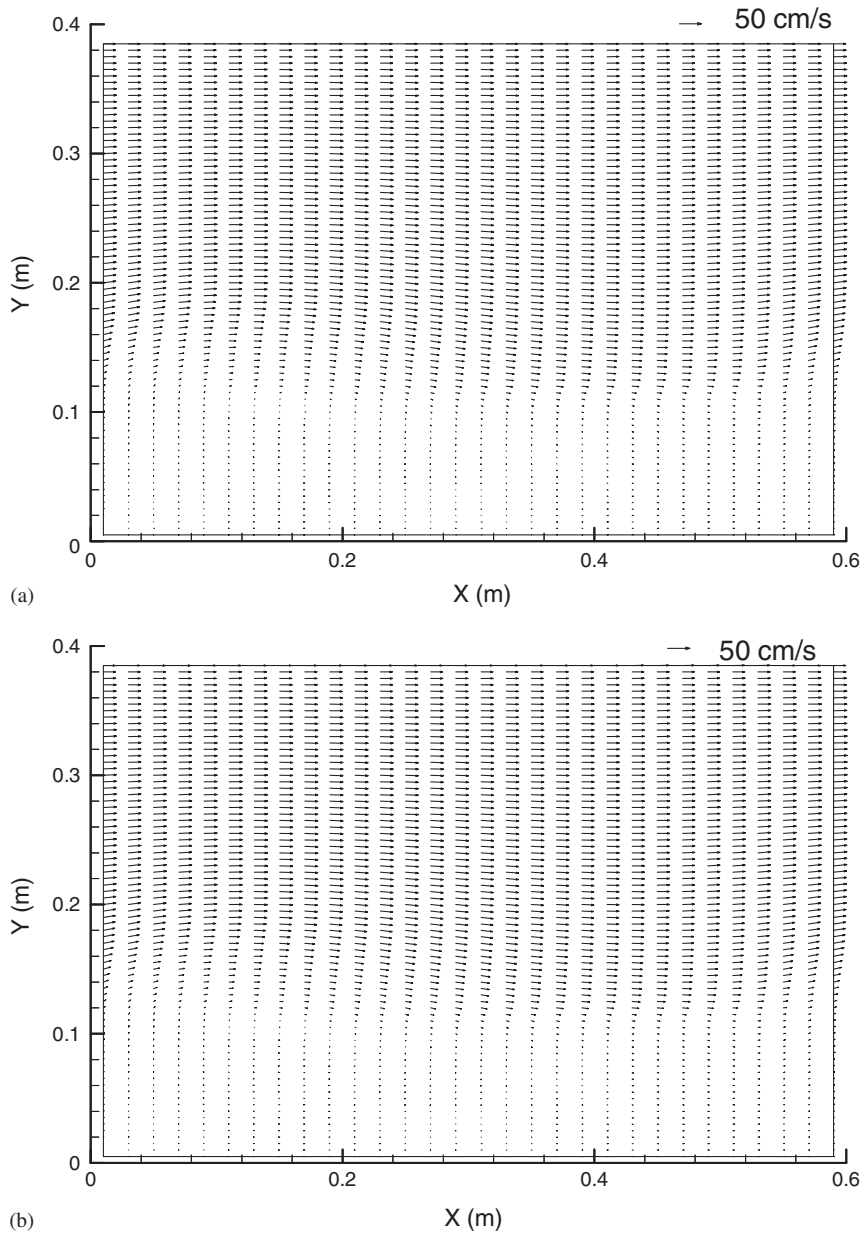

Figure 3. Velocity field for the initial development of a large eddy.

The present model can predict the vertical variation in velocity. Figure 9 displays the vertical velocity profiles in the main flow region and in the vegetated region. The logarithmic velocity distribution due to bottom roughness is satisfactorily reproduced in the main flow region. In the vegetated region, the resistance offered by the vegetation, which is proportional

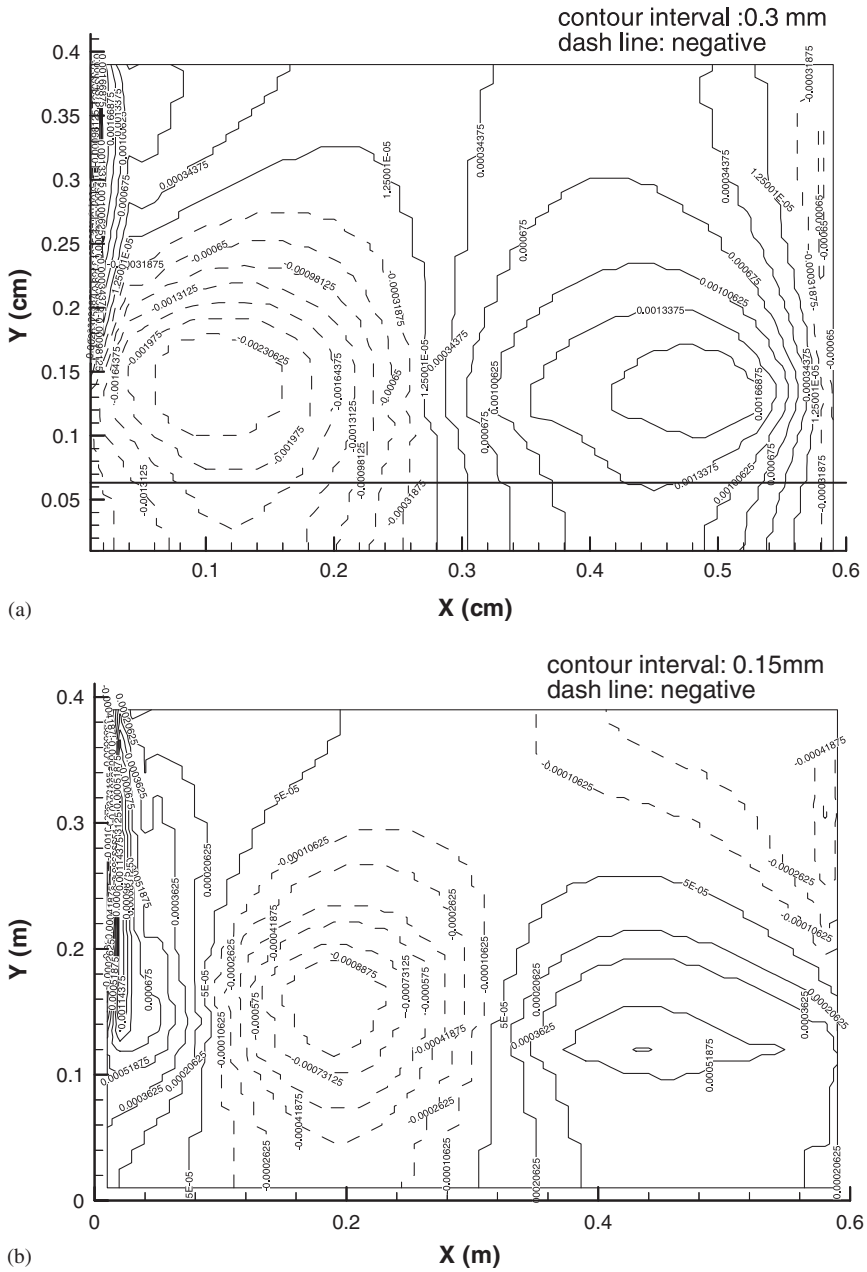

Figure 4. Spatial distribution of water surface elevation.

to the square of the velocity, causes a significant reduction in the flow resulting in a more or less uniform vertical distribution of velocity. Near the bed both the bottom friction and the resistance due to vegetation exert significant effects and a stagnation zone of velocity is resulted.

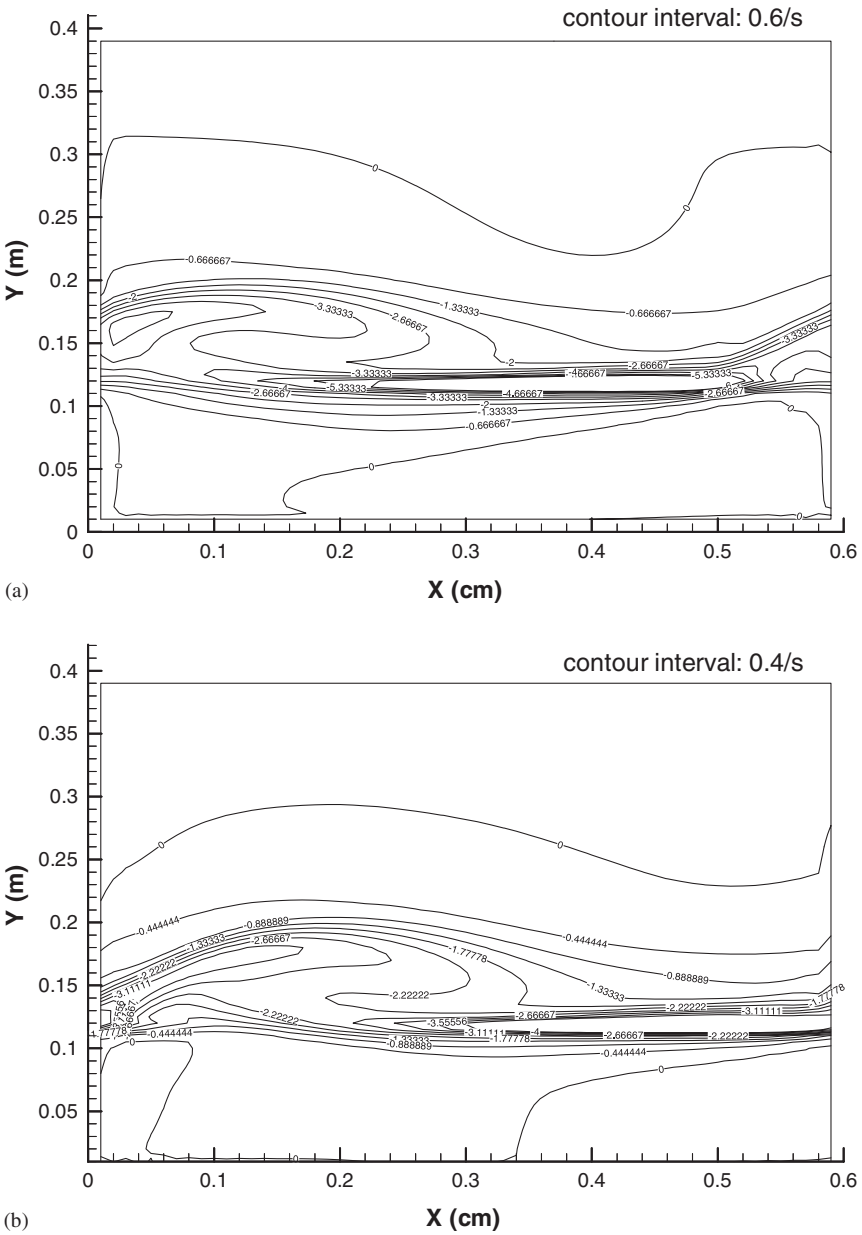

Figure 5. Spatial distribution of vorticity field.

Figure 10 shows the transverse distribution of the Reynolds stress $\overline{u_1', u_2'}$ for the two cases. Although, there is a small difference between the computed maximum stress and the measured one, the profile of the stress and the location of the maximum stress are similar. The Reynolds

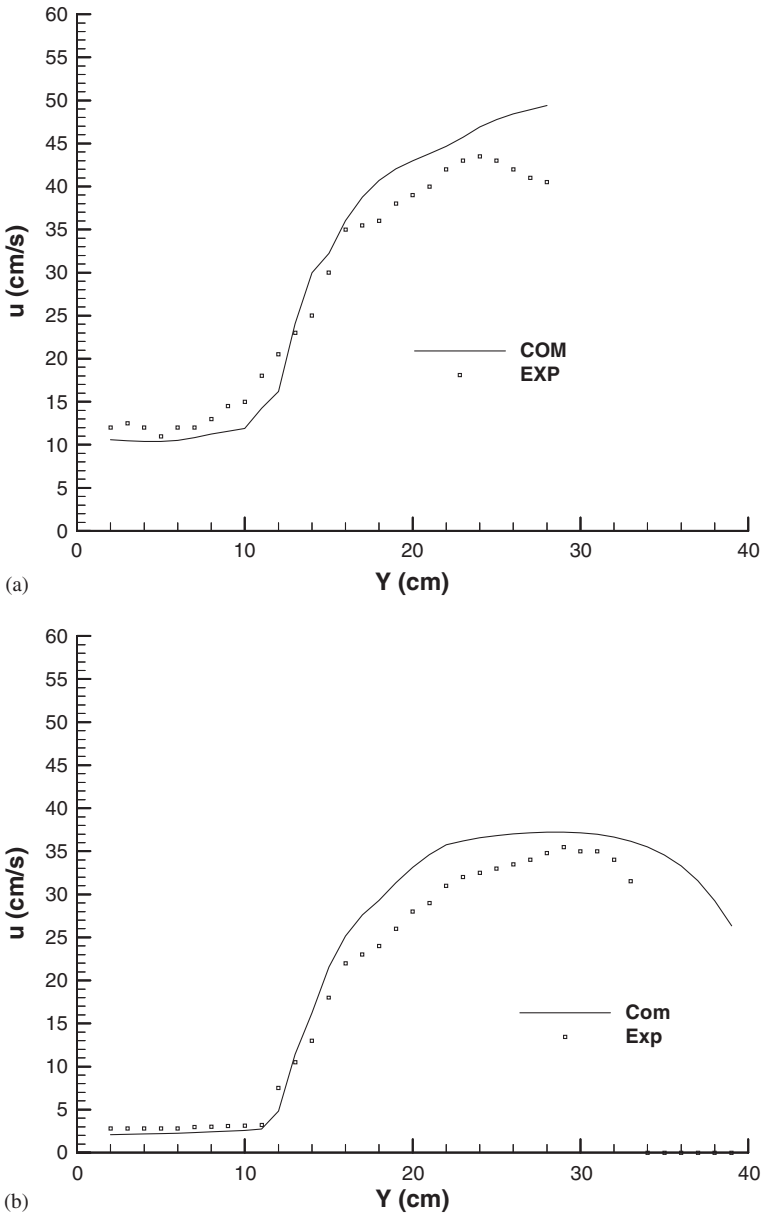

Figure 6. Transverse velocity profile (com: computed results; exp: experiment data from Tsujimoto and Kitamura [7]).

stress is obtained from the sum of the stress from large-scale term and that from the subgrid scale term. The contribution to Reynolds stress from the explicitly computed large-scale eddies is larger than that from the modelled subgrid scale eddies. The maximum of the Reynolds

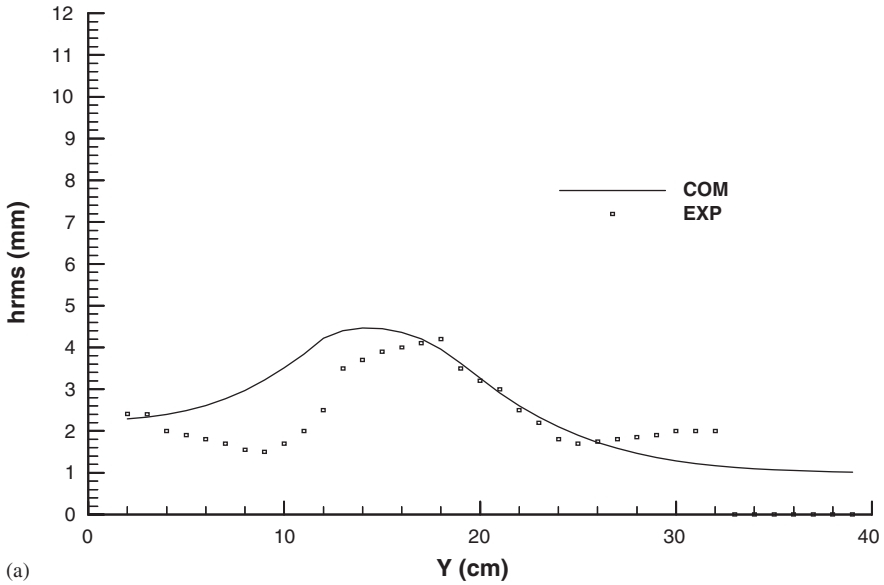

(a)

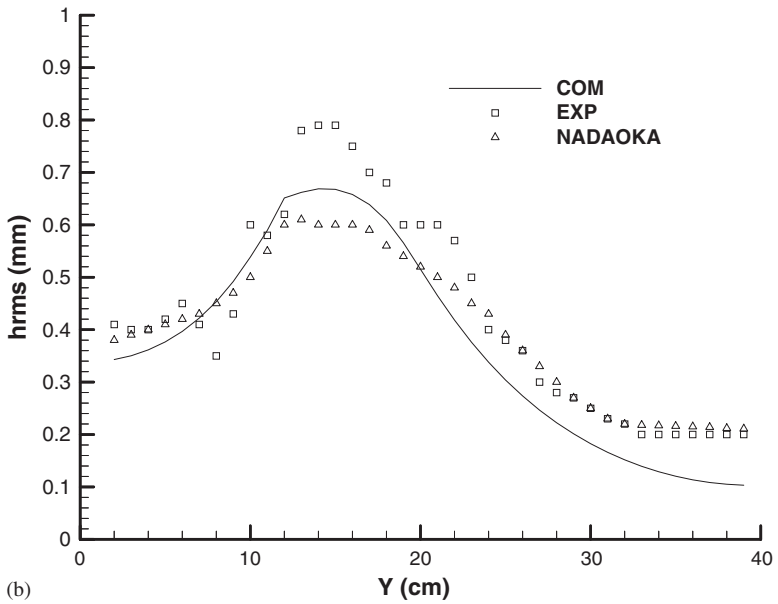

(b)

Figure 7. Temporal variation of water level fluctuation.

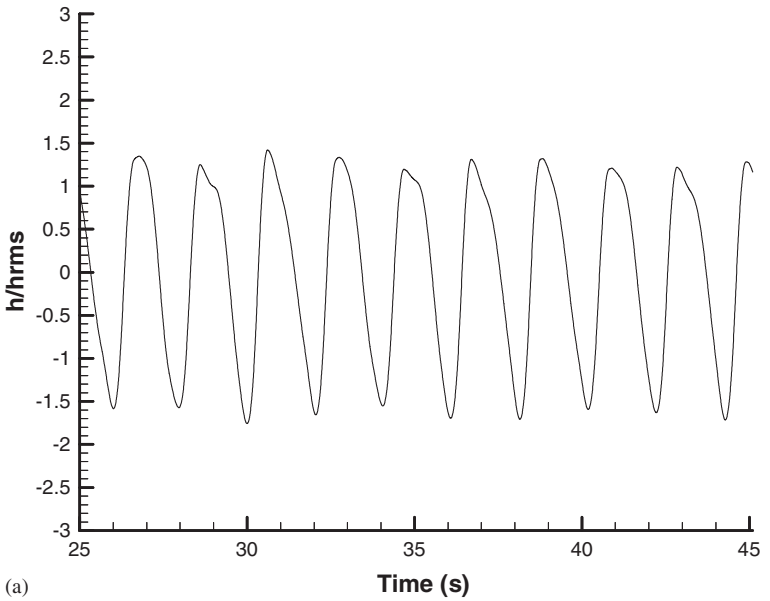

(a)

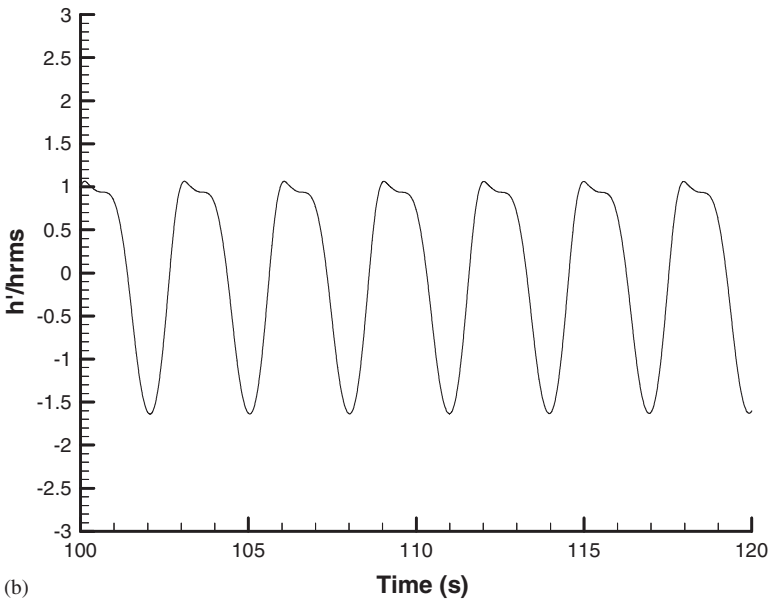

(b)

Figure 8. Root mean squares water level fluctuation (com: computed results; exp: experimental data from Tsujimoto and Kitamura [7]).

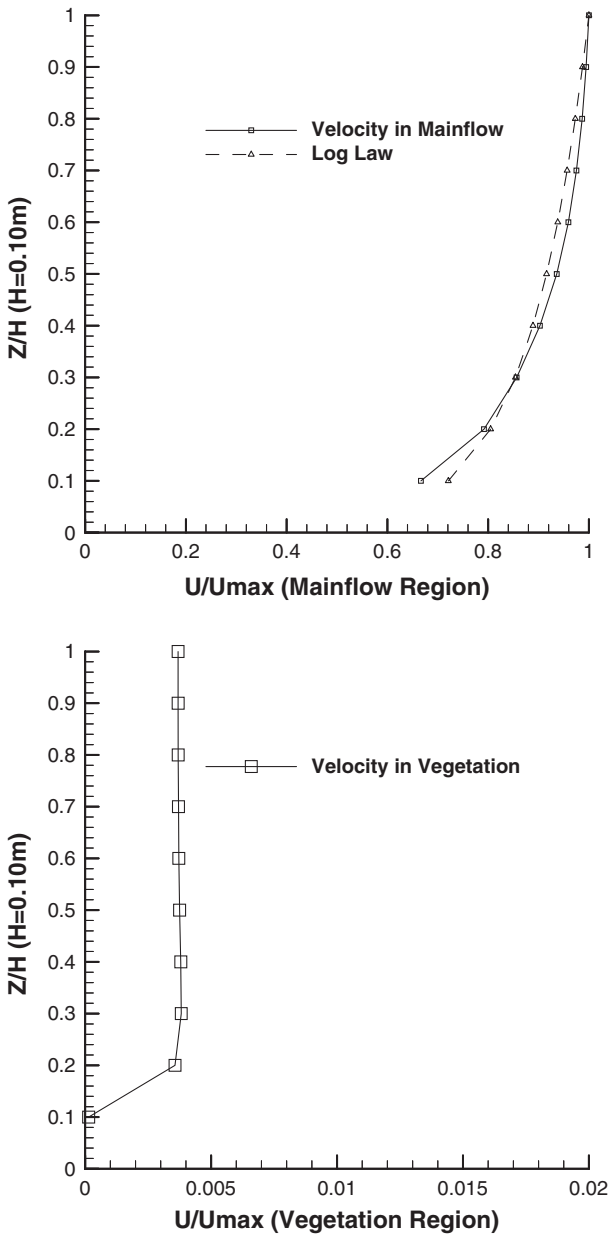

Figure 9. Vertical velocity profile: (a) main flow region; (b) vegetated region.

stress occurs at the interface where the velocity gradient is the greatest. Thus besides bottom friction, the vegetation resistance is another primary source of turbulent kinetic energy. The computed result from the present model is slightly better than the result from the SDS-2DH model.

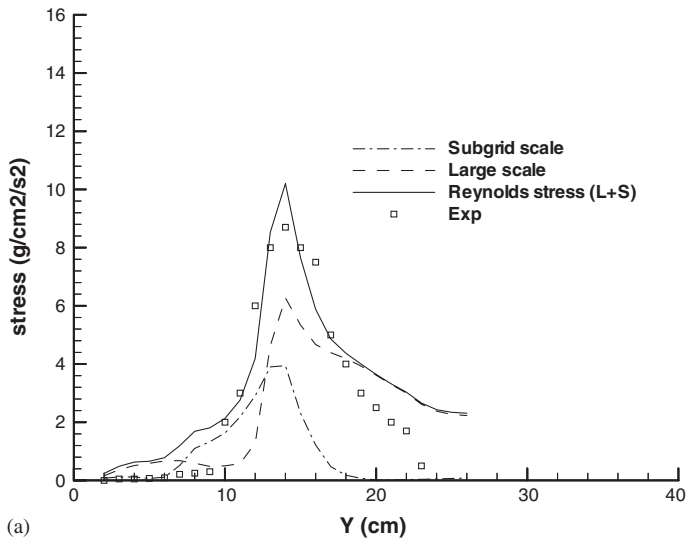

(a)

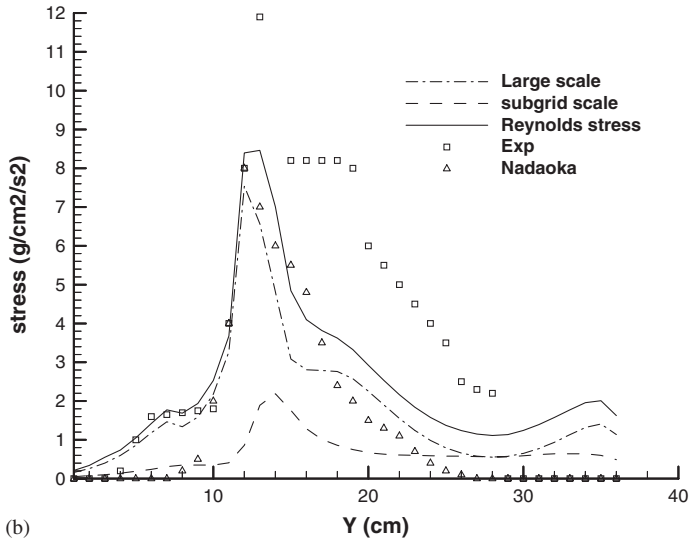

(b)

Figure 10. Transverse distribution of the Reynolds stress $\overline{u_1' u_2'}$ (exp: experimental data from Tsujimoto and Kitamura [7]).

CONCLUSIONS

A k–l LES model has been developed and applied to study the hydrodynamic behaviour of turbulent flow in a rectangular open channel containing a vegetated domain. An operator splitting method, which splits the solution procedure into advection, diffusion and pressure propagation steps, is used so that different numerical schemes can be used for the solution of different physical processes. The model has been validated for two cases of study and

good agreement between the computed results and experimental data has been attained. The results show that large eddies occur at the interface between the vegetated and non-vegetated domains, where significant mass and momentum exchange occurs. The profiles of velocity and stage of the channel flow are largely affected by the vegetation resistance. The logarithmic vertical velocity variation becomes uniform in the vegetated domain. The present k–l LES model is proven to be an useful tool for engineering applications.

ACKNOWLEDGEMENTS

This work was supported by a grant from the Research Grant Council of the Hong Kong Special Administrative Region (Project No. 5048/99E).

REFERENCES

1. Chow VT. *Open Channel Hydraulics*, McGraw Hill: New York, 1959.
2. Henderson FM. *Open Channel Flow*, MacMillan: New York, 1966.
3. Myers WRC, Elsawy EM. Boundary shear in channel with flood-plain. *Journal of Hydraulic Division*, *ASCE* 1975; **101**:933–946.
4. Zheleznyakov G. Relative deficit of mean velocity of instable river flow kinematic effects in river beds with flood plains. *Proceedings of the 11th IAHR-Congress*, Leningrad, subject 3.45, 1966.
5. Pasche E, Rouve G. Overbank flow with vegetatively roughened flood plains. *International Journal for Numerical Methods in Fluids* 1985; **111**:1262–1278.
6. Darby SE, Thorne CR. Predicting stage–discharge curves in channels with bank vegetation. *Journal of Hydraulic Engineering*, *ASCE* 1996; **122**:583–586.
7. Tsujimoto T, Kitamura T. Experimental study on open-channel flow with vegetated zone along side wall. *KHL Progressive Report* '92, Hydrology Laboratory, Kanazawa University, Japan, 1992; 21–35.
8. Tamai N, Asaeda T, Ikeda H. Study on generation of periodical large surface eddies in a composite channel flow. *Water Resources Research* 1986; **27**(7):1129–1138.
9. Fukuoka S, Fujita K. Flow resistance due to lateral momentum transport across vegetation in the river course. *Proceedings of the International Conference on Physical Modelling of Transport and Dispersion*, *ASCE*: 12B, New York, 1990; 25–30.
10. Chu VH, Wu JH, Khayat RE. Stability of transverse shear flows in shallow open channels. *Journal of Hydraulic Engineering*, *ASCE* 1991; **117**(10):1370–1381.
11. Ikeda S, Ohta K, Hasegawa H. Instability-induced horizontal vortices in shallow open-channel flows with an inflection point in skewed velocity profile. *Journal of Hydroscience and Hydraulic Engineering Techniques*, *Japan Society of Civil Engineers* 1994; **12**(2):69–84.
12. Thom AS. Momentum adsorption by vegetation. *Quarterly Journal of the Royal Meteorological Society* 1971; **97**:414–428.
13. Shaw RH, den Hartog G, King KM, Thurtell GW. Measurements of mean wind flow and three-dimensional turbulence intensity within a mature corn crop. *Agriculture Meteorology* 1974; **34**:419–425.
14. Oliver HR. Wind profiles in and above a forest canopy. *Quarterly Journal of the Royal Meteorological Society* 1971; **97**:548–553.
15. Kondo J, Akeshi S. Numerical studies of the two-dimensional flow in horizontally homogeneous canopy layers. *Boundary-Layer Meteorology* 1976; **10**:255–272.
16. Wilson NR, Shaw RH. A higher-order closure model for canopy flow. *Journal of Applied Meteorology* 1977; **16**:1197–1205.
17. Raupach MR, Tom AS. Turbulence in and above plant canopies. *Annual Review in Fluid Mechanics* 1981; **13**:97–129.
18. Burke RW, Stolzenbach KD. Free surface flow through salt marsh grass. *Report #MITSG* 83-16, Massachusetts Institute of Technology, 1983; 252.
19. Naot D, Nezu I, Nakagawa H. Hydrodynamic behaviour of partly vegetated open channels. *Journal of Hydraulic Engineering* 1996; **122**:625–633.
20. Shaw RH, Schumann U. Large-eddy simulation of turbulent flow above and within a forest. *Boundary-Layer Meteorology* 1992; **61**:47–64.
21. Patton EG, Shaw RH. Large-eddy simulation of windbreak flow. *Boundary-Layer Meteorology* 1998; **87**: 275–306.

22. Nadaoka K, Yagi H. Shallow-water turbulence modelling and horizontal large-eddy computation of river flow. *Journal of Hydraulic Engineering* 1998; **124**:493–500.
23. Li CW, Wang JH. Large eddy simulation of free surface shallow-water flow. *International Journal for Numerical Methods in Fluids* 2000; **34**(1):31–46.
24. Shimizu Y, Tsujimoto T. Comparison of Flood-Flow Structure Between Compound Channel and Channel with Vegetated Zone. *Proc. 25th Congress of IAHAR*, Tokyo, Japan A-3-4, 1995, 97–104.
25. Shimizu Y, Tsujimoto T, Nakagaea H. Numerical study on fully developed turblent flow in vegeted and non-vegetated zones in a cross-section of open channel. *Proc. Hydraulic Engrg.*, *JSCE*, 1992; **36**:265–272.
26. Schlichting H. *Boundary Layer Theory*, 4th edn., McGraw-Hill: New York, 1962.
27. Yu TS, Li CW. Efficient higher-order backward characteristics schemes for transient advection. *International Journal for Numerical Methods in Fluids* 1994; **19**:997–1012.
28. Leonard BP. A stable and accurate convective modelling procedure based on quadratic upstream interpolation. *Computer Methods in Applied Mechanical Engineering* 1979; **19**:59–98.

